

TRNSYS simulation of solar chimney power plants with a heat storage layer

Fei CAO^{1,2,*}, Yufei MAO¹, Tianyu ZHU¹, Liang ZHAO²

¹College of Mechanical and Electrical Engineering, Hohai University, Changzhou, P.R. China

²State Key Laboratory of Multiphase Flow in Power Engineering, Xi'an Jiaotong University, Xi'an, P.R. China

Received: 20.12.2016

Accepted/Published Online: 20.10.2016

Final Version: 30.07.2017

Abstract: The transient performance of a solar chimney power plant (SCPP) with a heat storage layer is evaluated in the present study. A modified TRNSYS type is built. The ground temperature, wind velocity at the chimney inlet, and the power capacity over two typical days are simulated and compared with and without considering the heat storage layer. SCPP performances with six ground materials (granite, limestone, sandstone, sand, wet soil, and water) are compared. The parameters are postponed for 2–3 h when the heat storage layer is considered. This is the multieffect of solar irradiation, air characteristics, and ambient temperature. The SCPP with sand as the heat storage layer material holds the best performance in the daytime and night. Considering its abundant distribution, ease of acquisition, cheap cost, and high performance, sand is suggested as the ground material for SCPPs.

Key words: Solar chimney power plant, solar chimney, heat storage, TRNSYS simulation

1. Introduction

The solar chimney power plant (SCPP) consists of three essential components: a solar collector, a chimney, and a group of turbine generators (Figure 1). The SCPP runs under the control of greenhouse and buoyance effects. The sunlight transfers through the collector cover and heats the heat storage layer below. The temperature of the heat storage layer increases and leads to a temperature difference between it and the air in the solar collector, and under this condition the heat convection occurs. The air in the solar collector is heated by the heat storage layer, which would cause a density difference between the air in the solar collector and in the chimney. Under the control of buoyancy effect, the air in the solar collector flows toward the chimney. The ambient cold air enters into the solar collector through the open edge, then flows into the chimney, and finally flows out from the chimney outlet, and so forth.

Commercial SCPPs contain huge areas of solar collectors, whose diameters are several kilometers [1–3]. According to the heat transfer progress, the heat storage layer has an important role in the SCPP. Previous studies have analyzed the influences of the heat storage layer, namely the material, absorptivity, and emissivity, on SCPP performance [2]. However, the heat storage layer was not well defined from transient points of view [2,4]. In the present study, a modified type in TRNSYS software is first developed, in which the heat storage layer is taken into account. The ground temperature, the wind velocity, and the power capacity are then analyzed by considering SCPP performance on typical days. Wind velocity and power efficiencies of six kinds of heat storage layer materials are also compared.

*Correspondence: yq.cao@hotmail.com

2. Mathematical model

A transient mathematical model is built for the SSCP. The mathematical model can be divided into three parts, namely the solar collector model, the chimney model, and the power conversion unit (PCU) model. Considering the symmetrical structure of the SSCP, the 3D geometry of the SSCP can be dimensionally reduced into a 2D structure (Figure 2). The coordinates of the mathematical model are established according to Figure 2. Practically, the SSCP has a large collector radius, high chimney, and large airflow velocity, compared with which the collector height, the collector cover thickness, and the temperature increase in the solar collector are much smaller [5–7]. Correspondingly, six assumptions are adopted to simplify the mathematical model: (1) temperature rises linearly along the r direction in the solar collector [8]; (2) ignore the velocity and temperature gradient in the z direction in the solar collector; (3) Boussinesq assumption is valid for the chimney [9–12]; (4) ignore the velocity and temperature gradient in the r direction in the chimney; (5) ignore the temperature difference between the collector upper and back surface, and (6) airflow is under adiabatic conditions in the chimney.

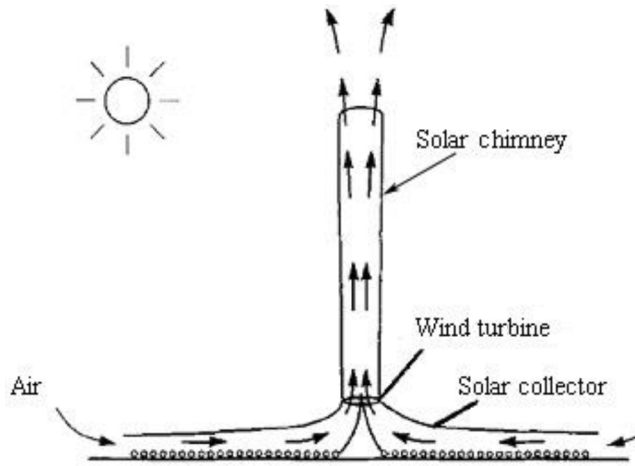


Figure 1. Schematic of an SSCP.

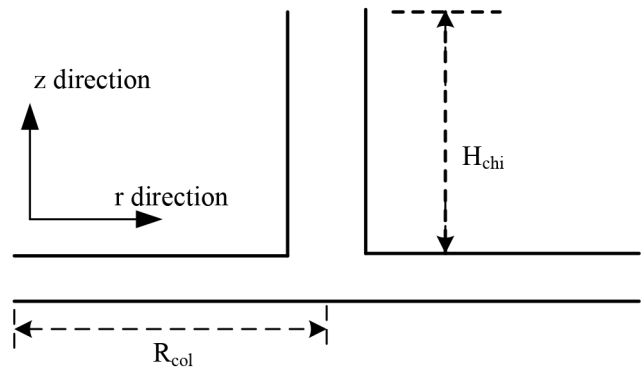


Figure 2. Coordinates of the simplified SSCP model.

2.1. Solar collector

Continuity equation:

$$\frac{\partial \rho}{\partial t} + \frac{1}{r} \frac{\partial}{\partial r} (\rho r v_r) = 0 \tag{1}$$

Momentum equation:

$$\frac{\partial}{\partial t} (\rho v_r) + \rho v_r \frac{\partial v_r}{\partial r} = -\frac{\partial p}{\partial r} + \mu \left[\frac{\partial}{\partial r} \left(\frac{1}{r} \frac{\partial}{\partial r} (r v_r) \right) \right] \tag{2}$$

Energy equation:

$$\frac{\partial}{\partial t} (\rho c_p T) + \frac{\partial}{\partial r} (c_p \rho v_r T) = \frac{\partial S_\Phi}{\partial t} \tag{3}$$

Considering the energy balance of a representative elemental volume, as shown in Figure 3, the energy source $\partial S_\Phi / \partial t$ is

$$\frac{\partial S_\Phi}{\partial t} = q_{cf} r \Delta \theta \Delta r + q_{gf} r \Delta \theta \Delta r + \rho_f c_{p,f} \frac{\partial T_f}{\partial t} H r \Delta \theta \Delta r, \tag{4}$$

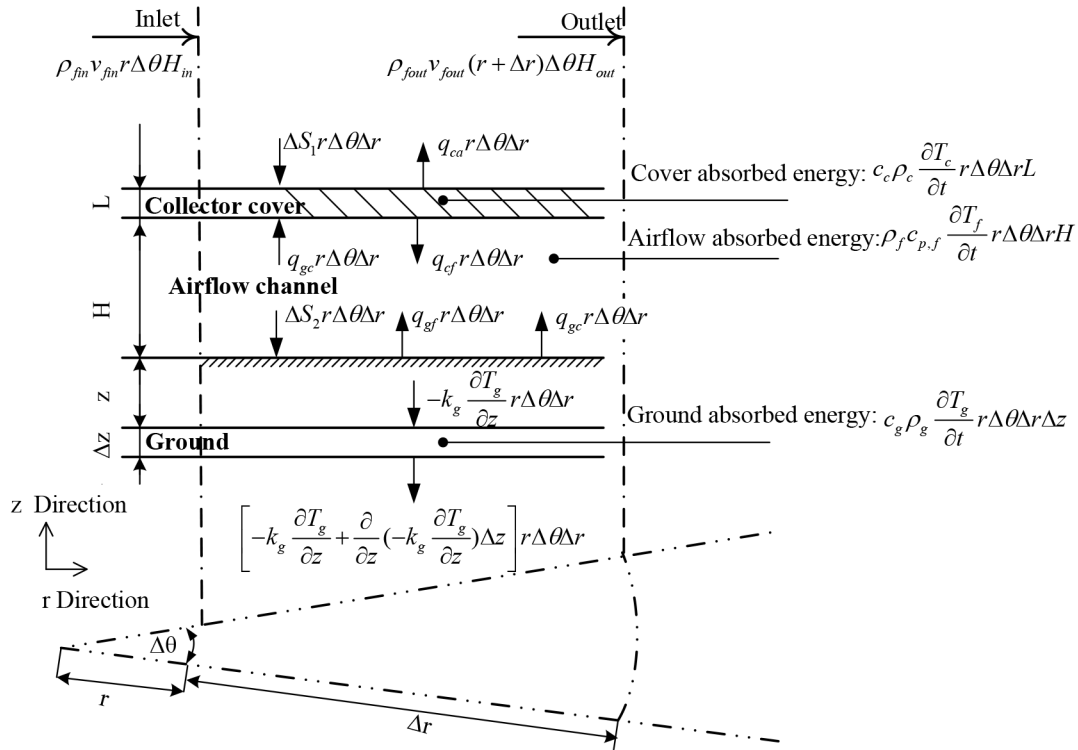


Figure 3. Energy balance of a representative elemental volume in the solar collector.

where the first and the second terms on the right side of Eq. (4) are the heat exchange between the collector cover and airflow and between the ground and the airflow, which can be expressed as

$$q_{cf} r \Delta \theta \Delta r = \frac{\partial S_1}{\partial t} r \Delta \theta \Delta r + q_{gc} r \Delta \theta \Delta r - q_{ca} r \Delta \theta \Delta r - c_c \rho_c \frac{\partial T_c}{\partial t} r \Delta \theta \Delta r L, \tag{5}$$

$$q_{gf} r \Delta \theta \Delta r = \frac{\partial S_2}{\partial t} r \Delta \theta \Delta r + k_g \frac{\partial T_g}{\partial z} \Big|_{z=0} r \Delta \theta \Delta r - q_{gc} r \Delta \theta \Delta r, \tag{6}$$

where $q_{gc} r \Delta \theta \Delta r$ is the radiation heat exchange between the ground and the collector cover, $q_{ca} r \Delta \theta \Delta r$ is the convection and radiation heat exchange between the collector cover and the ambient, and $k_g \frac{\partial T_g}{\partial z} \Big|_{z=0} r \Delta \theta \Delta r$ is the heat contribution from the ground. Taking a depth of Δz into consideration, we obtain

$$-k_g \frac{\partial T_g}{\partial z} r \Delta \theta \Delta r \Delta z = \left[-k_g \frac{\partial T_g}{\partial z} + \frac{\partial}{\partial z} \left(-k_g \frac{\partial T_g}{\partial z} \right) \Delta z \right] r \Delta \theta \Delta r \Delta z + c_g \rho_g \frac{\partial T_g}{\partial t} r \Delta \theta \Delta r \Delta z \tag{7}$$

Integrating Eqs. (1)–(7) along directions r , θ , and z , the energy balance of the solar collector in the time period of Δt is obtained.

2.2. Chimney

Continuity equation:

$$\frac{\partial \rho}{\partial t} + \frac{\partial}{\partial z} (\rho v_z) = 0 \tag{8}$$

Momentum equation:

$$\frac{\partial}{\partial t}(\rho v_z) + \rho v_z \frac{\partial v_z}{\partial z} = -\frac{\partial p}{\partial z} - \rho g_z + \mu \frac{\partial^2 v_z}{\partial z^2} \quad (9)$$

Energy equation:

$$\frac{\partial}{\partial t}(c_p \rho T) + \frac{\partial}{\partial z}(c_p \rho v_z T) = 0 \quad (10)$$

According to the Boussinesq assumption, the momentum equation of the chimney can be simplified as

$$-\frac{\partial p}{\partial z} - \rho g_z + \mu \frac{\partial^2 v_z}{\partial z^2} = 0 \quad (11)$$

2.3. PCU

As the connection section of the PCU is irregular, a randomized coordinate along the power generator surface l is built for this area (Figure 4). We can obtain

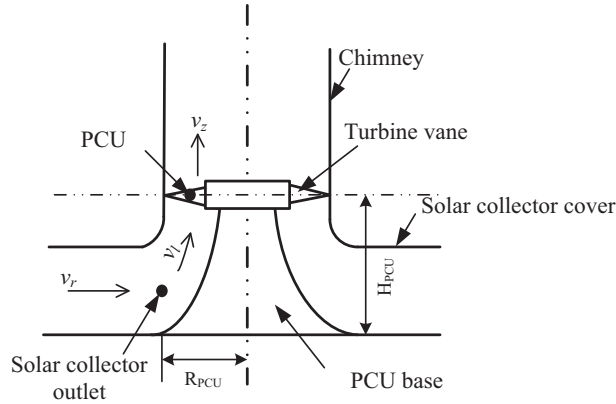


Figure 4. Cross-section of the PCU.

Continuity equation:

$$\frac{\partial \rho}{\partial t} + \frac{\partial}{\partial l}(\rho v_l) = 0 \quad (12)$$

Momentum equation:

$$\frac{\partial}{\partial t}(\rho v_l) + \rho v_l \frac{\partial v_l}{\partial l} = -\frac{\partial p}{\partial l} - \rho g_l + \mu \frac{\partial^2 v_l}{\partial l^2} \quad (13)$$

Energy equation:

$$\frac{\partial}{\partial t}(c_p \rho T) + \frac{\partial}{\partial l}(c_p \rho v_l T) = \frac{\partial}{\partial l} \left(k \frac{\partial T}{\partial l} \right) \quad (14)$$

As $H_{PCU} \ll H_{chi}$ and $R_{PCU} \ll R_{col}$, we can obtain

$$v_r |_{r=R_{PCU}} = v_l |_{l=0} \quad (15)$$

$$v_z |_{z=H_{PCU}} = v_l |_{l=L_{PCU}} \quad (16)$$

$$H_{PCU} \approx 0, \quad (17)$$

where H_{chi} is the chimney height, R_{col} is the collector radius, and L_{PCU} is the length of the PCU channel.

Consequently, the momentum equation can be simplified as

$$-\frac{\partial p}{\partial l} + \mu \frac{\partial^2 v_l}{\partial l^2} = 0 \tag{18}$$

2.4. Coefficients and power generation

The generated pressure is consumed by four parts, namely the friction losses in the collector and the chimney (ΔP_f), the kinetic energy losses at the turbine inlet (ΔP_{in}), the kinetic energy losses at the chimney outlet (ΔP_{out}), and the rest is the effective pressure used by the turbine to generate electricity (ΔP_t).

$$\begin{aligned} \Delta P_{tot} &= \Delta P_f + \Delta P_{in} + \Delta P_{out} + \Delta P_t \\ &= f \frac{L_{th}}{D} \frac{1}{2} \rho_f v_f^2 + \gamma \frac{1}{2} \rho_o v_o^2 + \frac{1}{2} \rho_{out} v_{out}^2 + \Delta P_t \end{aligned} \tag{19}$$

The power generated by the turbine (P_{ele}) is

$$P_{ele} = \eta_t \Delta P_t v_l A_{chi}, \tag{20}$$

where η_t is the turbine efficiency and A_{chi} is the chimney cross-section area.

Equations to calculate the coefficients (the heat transfer coefficients among the collector cover, the airflow and the ground, the collector cover loss coefficients, the ground loss coefficients, the friction loss, turbine efficiency, etc.) follow the published literature [4,13,14]. The equations are converted into codes in Fortran and coupled into the TRNSYS program to build a new Type-SCPP according to the method in our previous study [13,14]. The new Type-SCPP is then used to simulate the transient performance of the SCPP. Weather parameters are supplied by the TRNSYS Type 15-2, which supplies typical meteorological year data.

3. Results and discussion

The configuration sizes and parameters required in the TRNSYS Type are shown in the Table. The SCPPs are located in Lanzhou, a typical city in northwest China.

Table. Configuration and parameters of the SCPP.

Component	Parameter	SCPP
Solar Collector	Collector radius	550 m
	Collector area	950,000 m ²
	Collector height	0 m
Chimney	Chimney height	547 m
	Chimney diameter	54 m
Ground	Ground material	Granite
	Reflectivity	0.25
Turbine generator	Efficiency	0.8
	Inlet loss	0.056

The solar radiation, ambient temperature, and ground temperature of the SCPP with and without considering the heat storage layer are shown in Figure 5. Similar tendencies are found between the solar

radiation and the ambient and the ground temperature without considering the heat storage layer, but the ground temperature of the SCPP when considering the heat storage layer is a little less than without considering the heat storage layer. Moreover, the ground temperature peak is postponed for about 2 h. When solar radiation is absorbed by the ground, the absorbed heat is consumed by the air, the collector cover, and the ground. In day 2 of Figure 5, the solar radiation increases from 0900 to 1300 hours; hence the ground temperature and the ambient temperature also increase in the time period. However, from 1300 to 1500 hours, the incident solar radiation decreases, as the solar radiation consumed by the air and the deeper ground is less than the incidental solar radiation. The ground temperature during this time period increases as well. Correspondingly, the incidental solar radiation cannot afford the air and deeper ground consumed energy, and the ground temperature after 1500 hours decreases gradually. This also explains why the solar radiation fluctuates during 1200 to 1400 hours but the ground temperature increase steadily during this period.

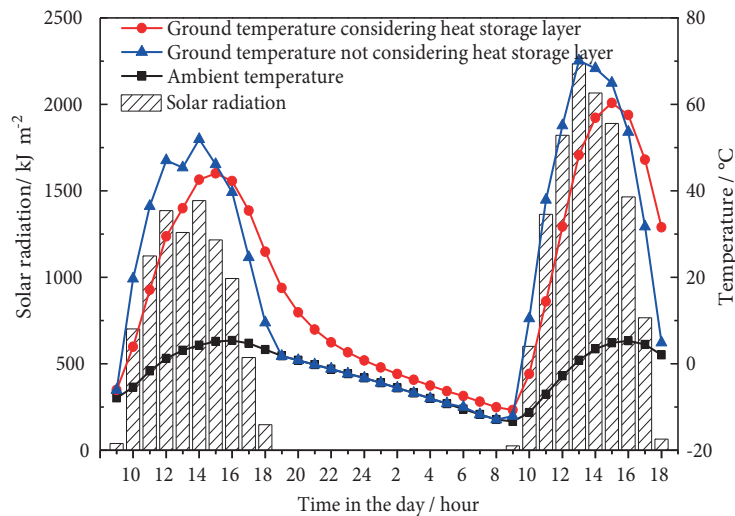


Figure 5. The ambient temperature and ground temperature of the SCPP over two typical days.

The wind velocity of the SCPP with and without considering the heat storage layer is shown in Figure 6. As no solar radiation is absorbed by the solar collector at night, no wind velocity is observed for the SCPP without considering the heat storage layer. However, the practical wind velocity at night is relatively high. In the daytime, the wind velocity curve is postponed for about 3 h from the solar radiation curve. Small solar radiation fluctuation has little effect on the wind velocity when solar radiation is abundant. In the night, the wind velocity decreases gradually to one-third of the maximum wind velocity. The wind velocity is a multiresult of the solar radiation, air characteristics, and the ambient temperature. In order to find the influence of the heat storage layer effect, the wind velocity at the chimney inlet (assuming that the heat in the storage layer releases gradually) is also shown in Figure 6. More than 30 h is needed to release the heat totally from the storage layer. Thus, the heat storage layer cannot release the heat totally during the night.

Power capacity of the SCPP with and without considering the heat storage layer is shown in Figure 7. As expected, the power capacity curves have similar tendencies to the wind velocity curves. Though the wind velocity at the chimney inlet is relatively high at night, its power capacity is low. The reason is that the air density at night is greater than in the daytime (see Eqs. (11) and (20) for details).

The wind velocities of SCPP with different heat storage layer materials are then shown in Figure 8. Six kinds of ground materials are taken into account and their power efficiencies are diagrammed in Figure 9. The

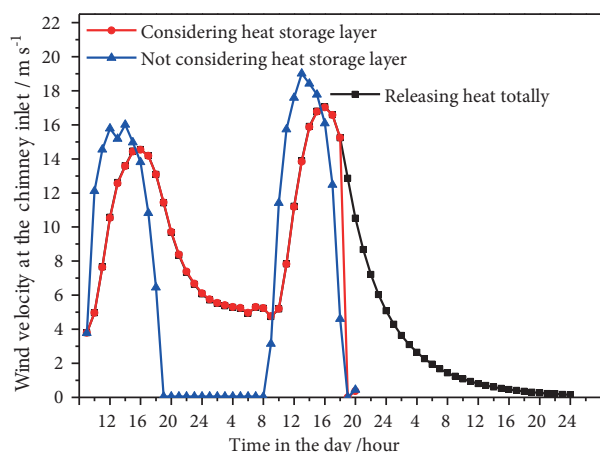


Figure 6. Wind velocity of the SCPP with and without considering the heat storage layer and under total heat release conditions.

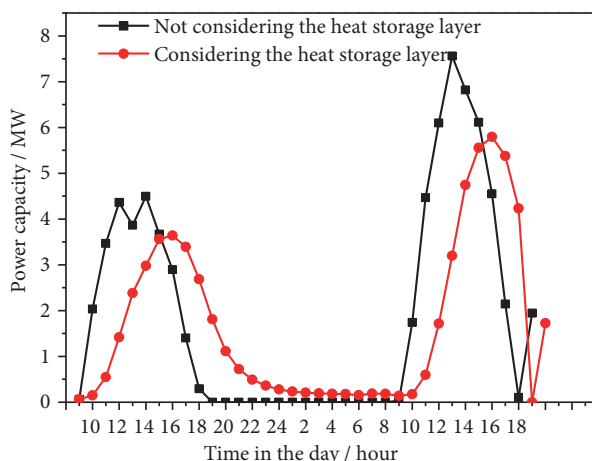


Figure 7. Power capacity of the SCPP with and without considering the heat storage layer.

SCPP with sand and wet soil as the heat storage layer generates the highest and lowest amounts of power in the daytime, respectively (Figure 8). The SCPP with water and sandstone as the heat storage layer generates the highest and lowest power in the night, respectively. The SCPP with sand as its heat storage layer holds the highest peak wind velocity and power efficiency in the two typical days (Figures 8 and 9). In addition, sand is cheap, abundant, and easy to obtain. Correspondingly, sand is recommended as the ground material.

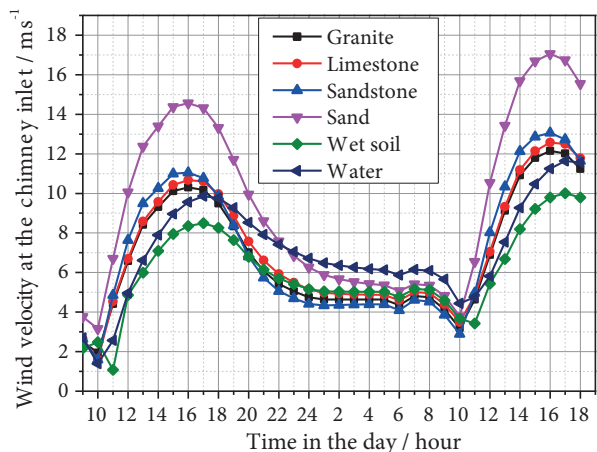


Figure 8. Wind velocity of SCPP with different heat storage layer materials.

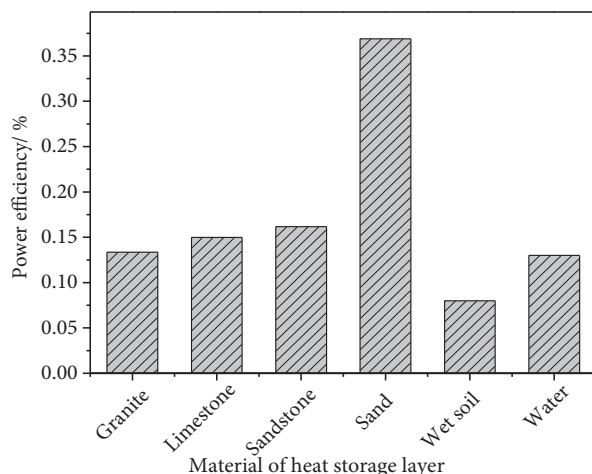


Figure 9. Power efficiency of SCPP with different heat storage layer materials.

4. Conclusions

The heat storage layer plays an important role in SCPP performance. A modified Type in TRNSYS software is developed, aiming to simulate the ground temperature, the wind velocity, and the power capacity of SCPPs with different heat storage layer materials. In this study, it was found that:

1. The ground temperature of the SCPP when considering the heat storage layer is a little lower than without considering the heat storage layer. Its ground temperature peak is postponed for about 2 h.

2. The wind velocity is a multiresult of solar radiation, air characteristics, and the ambient temperature. The heat storage layer cannot release the heat totally during the night.
3. Among the six conventional heat storage materials (granite, sand, limestone, sandstone, wet soil, and water), sand is suggested as the heat storage material considering its high performance and ease of acquisition.

Acknowledgments

This research was supported by the National Natural Science Foundation of China (No: 51506043), the Fundamental Research Funds for the Central Universities (No.: 2014B19714) and Jiangsu Province Science and Technology Support Plan Project (No: 862013070).

References

- [1] Zhou XP, Wang F, Ochieng RM. A review of solar chimney power technology. *Renew Sust Energy Rev* 2010; 14: 2315-2338.
- [2] Pretorius JP, Kroger DG. Sensitivity analysis of the operating and technical specifications of a solar chimney power plant. *J Sol Energ-T ASME* 2007; 129: 171-178.
- [3] Schlaich J. *The Solar Chimney: Electricity from the Sun*. Stuttgart, Germany: Axel Menges, 1995.
- [4] Cao F, Li HS, Zhao L, Bao TY, Guo LJ, Design and simulation of the solar chimney power plants with TRNSYS. *Sol Energy* 2013; 98: 23-33.
- [5] Haaf W, Friedrich K, Mayr G, Schlaich J. Solar chimneys. Part I: principle and construction of the pilot plant in Manzanares. *Int J Sol Energy* 1983; 2: 3-20.
- [6] Haaf W. Solar chimneys. Part II: preliminary test results from the Manzanares pilot plant. *Int J Sol Energy* 1984; 2: 141-161.
- [7] Roozbeh S. Performance evaluation of solar chimney power plants in Iran. *Renew Sust Energy Rev* 2012; 16: 704-710.
- [8] Bilgen E, Rheault J. Solar chimney power plants for high latitudes. *Sol Energy* 2005; 79: 449-458.
- [9] Schlaich J, Bergermann R, Schiel W, Weinrebe G. Design of commercial solar updraft tower systems - utilization of solar induced convective flows for power generation. *J Sol Energ-T ASME* 2005; 127: 117-124.
- [10] Kalash S, Naimeh W, Ajib S. Experimental investigation of the solar collector temperature field of a sloped solar updraft power plant prototype. *Sol Energy* 2013; 98: 70-77.
- [11] Fan J, Furbo S. Buoyancy effects on thermal behavior of a flat-plate solar collector. *J Sol Energ-T ASME* 2008; 130: 021010.
- [12] Pasumarthi N, Sherif SA. Experimental and theoretical performance of a demonstration solar chimney model, part I: mathematical model development. *Int J Energy Res* 1998; 22: 277-288.
- [13] Cao F, Li HS, Ma QM, Zhao L. Design and simulation of a geothermal-solar combined chimney power plant. *Energy Convers Manage* 2014; 84: 186-195.
- [14] Cao F, Zhao L, Guo, LJ. Simulation of a sloped solar chimney power plant in Lanzhou. *Energy Convers Manage* 2011; 52: 2360-2366.